4D cell biology: big data image analytics and lattice light-sheet imaging reveal dynamics of clathrin-mediated endocytosis in stem cell–derived intestinal organoids

Johannes Schöneberg[a], Daphné Dambournet[a], Tsung-Li Liu[b], Ryan Forster[a], Dirk Hockemeyer[a], Eric Betzig[a,b,c], and David G. Drubin[a,*]

[a]Department of Molecular and Cell Biology and [c]Department of Physics, University of California, Berkeley, Berkeley, CA 94720; [b]Janelia Research Campus, Howard Hughes Medical Institute, Ashburn, VA 20147

ABSTRACT **New methods in stem cell 3D organoid tissue culture, advanced imaging, and big data image analytics now allow tissue-scale 4D cell biology, but currently available analytical pipelines are inadequate for handing and analyzing the resulting gigabytes and terabytes of high-content imaging data. We expressed fluorescent protein fusions of clathrin and dynamin2 at endogenous levels in genome-edited human embryonic stem cells (hESCs), which were differentiated into hESC-derived intestinal epithelial organoids. Lattice light-sheet imaging with adaptive optics (AO-LLSM) allowed us to image large volumes of these organoids (70 × 60 × 40 µm *xyz*) at 5.7 s/frame. We developed an open-source data analysis package termed pyLattice to process the resulting large (~60 GB) movie data sets and to track clathrin-mediated endocytosis (CME) events. CME tracks could be recorded from ~35 cells at a time, resulting in ~4000 processed tracks per movie. On the basis of their localization in the organoid, we classified CME tracks into apical, lateral, and basal events and found that CME dynamics is similar for all three classes, despite reported differences in membrane tension. pyLattice coupled with AO-LLSM makes possible quantitative high temporal and spatial resolution analysis of subcellular events within tissues.**

Monitoring Editor
Diane Barber
University of California, San Francisco

Received: Jun 18, 2018
Revised: Aug 28, 2018
Accepted: Sep 1, 2018

INTRODUCTION

Quantitative cell biology aims to understand cellular processes by studying cells and tissues under conditions that recapitulate the in vivo environment as closely as possible. Recent advances in the fields of 1) stem cells and 3D organoid culture (Figure 1A), 2) advanced fluorescence imaging (Figure 1B), and 3) big data image analytics (Figure 1C) are now coming together to unlock a new level of temporal and spatial detail for this research: 4D cell biology. In this article we present the development of critical software and technology to enable 4D cell biology and describe how we applied it to investigate clathrin-mediated endocytosis (CME).

Stem cell and intestinal organoid technologies have advanced rapidly since the intestinal stem cell was first validated by in vivo lineage tracing (Barker *et al.*, 2007), and in vitro intestinal organoid culture systems were first reported in 2009 (Ootani *et al.*, 2009; Sato *et al.*, 2009). While the first of these cultures were derived from animal models, they can now also be grown from human tissues, embryonic stem cells, and induced pluripotent stem cells (iPSCs) (Sato *et al.*, 2011; Spence *et al.*, 2011; Forster *et al.*, 2014; McCracken *et al.*, 2014; Crespo *et al.*, 2017). Today, stem cells can be differentiated into tissues as diverse and complicated as taste buds, stomach, liver, pancreas, inner ear, kidney, and brain (Fatehullah *et al.*, 2016). Organoids differ from tissue aggregates and cocultures in that they contain multiple cell types that develop from stem cells or organ progenitors and comprise lineage-committed cells that self-organize and possess some function of the respective tissue in vivo (Lancaster and Knoblich, 2014). These organoids, and 3D tissue culture

This article was published online ahead of print in MBoC in Press (http://www.molbiolcell.org/cgi/doi/10.1091/mbc.E18-06-0375) on September 6, 2018.

*Address correspondence to: David G. Drubin (drubin@berkeley.edu).

Abbreviations used: 2D, two dimensional (*xy*); 3D, three dimensional (*xyz*); 4D, four dimensional (*xyz* and time); AO-LLSM, adaptive optics lattice light-sheet microscope; Cltr, clathrin; CME, clathrin-mediated endocytosis; DMSO, dimethyl sulfoxide; Dnm2, dynamin2; EGF, epidermal growth factor; hESC, human embryonic stem cells; iPSC, induced pluripotent stem cell; LLSM, lattice light-sheet microscope; MDCK, Madin–Darby canine kidney; TIRFM, total internal reflection fluorescence microscopy.

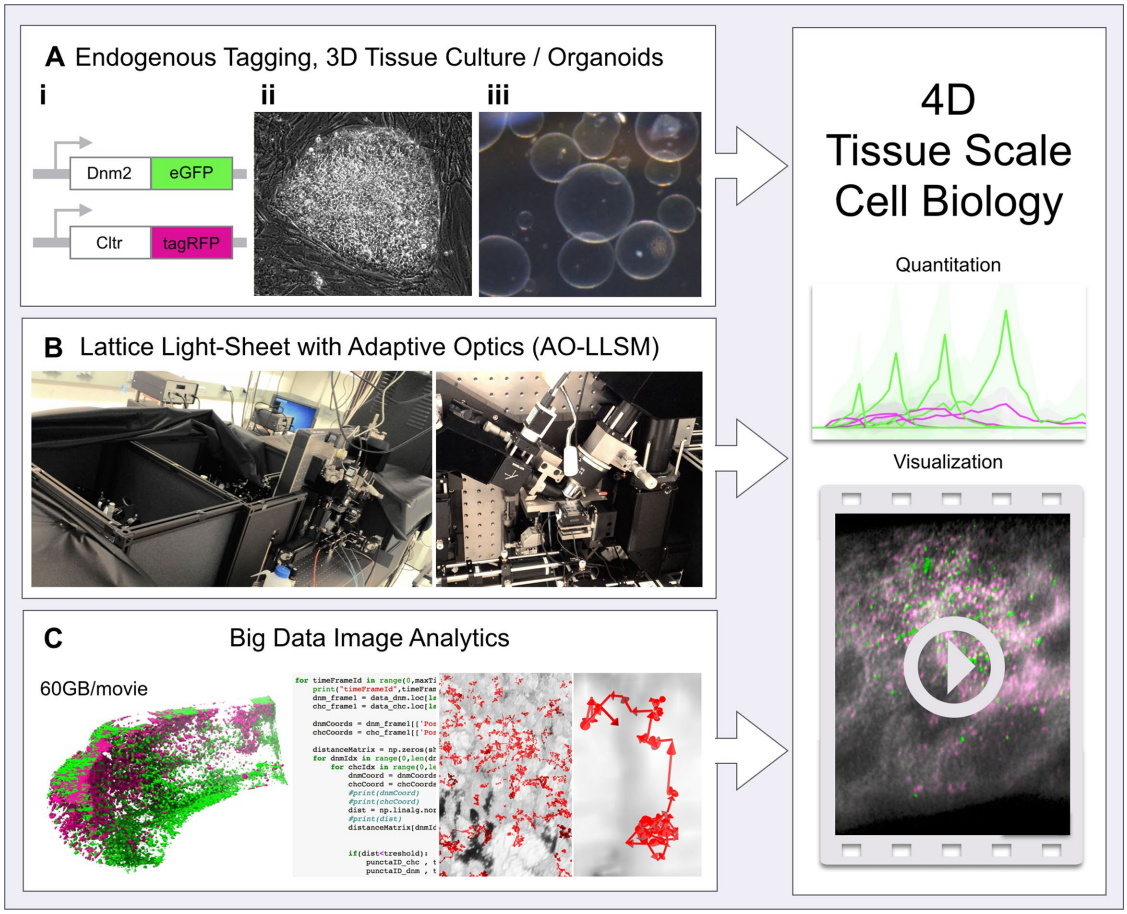

FIGURE 1: (Left) A new level of 4D tissue cell biology is unlocked as recent advances from three fields come together: (A) endogenous protein tagging using genome editing (i), stem cell biology (ii), and 3D tissue/organoid culture (iii); (B) 4D noninvasive advanced fluorescence imaging with a lattice light-sheet microscope with adaptive optics (AO-LLSM; left: full view of the microscope; right: focus on the characteristic objective arrangement); and (C) advances and software in big data image analytics. (Right) Combination of these elements allows unprecedented quantitative analysis of subcellular events within live tissues in 4D.

methods in general, allow unprecedented research opportunities by bringing research away from individual cells or layers of cells grown on a plastic or glass surface and toward differentiated 3D tissues, as reviewed in Clevers (2016).

While organoids have allowed cell culture to move into the third dimension with live 3D tissue cultures, imaging these cultures using existing approaches to microscopy remained challenging. Conventional fluorescence microscopy has been an indispensable tool for studying cell biology, but has had severe limitations. For example, laser powers required for sensitive imaging in confocal microscopy can cause bleaching and phototoxicity, which limits live cell imaging to low frame rates, short observation times, and imaging in a single plane (2D). The recent advent of lattice light-sheet microscopy (LLSM) (Chen *et al.*, 2014) addresses these limitations: extremely fast image acquisition and low phototoxicity allow nearly bleaching-free imaging of live cells for tens of minutes in 3D. Importantly, the recent combination of adaptive optics with lattice light-sheet technology (AO-LLSM) (Liu *et al.*, 2018) is ideally suited for tissue imaging tasks, as tissue-induced aberrations can be corrected, resulting in 4D movies (three space dimensions and time) with previously unachievable clarity.

With live 3D organoid cultures and the possibility of imaging them in 4D using AO-LLSM, only one challenge remains: the large amounts of data generated by the novel imaging technique. Semi-manual analysis, as is usually done for 2D data sets that are in the size range of hundreds of megabytes, such as through ImageJ/Fiji (Schindelin *et al.*, 2012; Rueden *et al.*, 2017), becomes prohibitive for the gigabytes and terabytes of 4D imaging data sets. Sophisticated analysis algorithms (Jaqaman *et al.*, 2008; Aguet *et al.*, 2016) and 4D visualization tools (Goddard *et al.*, 2018) are required, as well as new thinking about data storage (Cheeseman *et al.*, 2018) and how best to apply machine learning (Hong *et al.*, 2015; Ounkomol *et al.*, 2018). In this paper, existing tools were adapted and paired with new code, resulting in the *pyLattice* package. Building on a core of proven particle-tracking tools (Jaqaman *et al.*, 2008; Aguet *et al.*, 2016), pyLattice operates on the widely used open-source scientific computing framework Jupyter (Perez and Granger, 2007) and interfaces with the novel open-source 4D LLSM viewer ChimeraX (Goddard *et al.*, 2018). The resulting code features a user-friendly Python interface, support for large AO-LLSM data sets, and support for membrane detection, membrane classification into basal, apical, and lateral, and assignment of molecule detections to these specific membranes. pyLattice is open source and aims to be a general tool for 4D LLSM data analytics.

We used all three aspects of 4D cell biology (3D tissue culture, 4D imaging, and advanced image analytics) to study clathrin-mediated endocytosis (CME). CME is an ubiquitous and essential process in the cell that controls lipid homeostasis, receptor internalization, and cell signaling (Kaksonen and Roux, 2018). The pathway involves the

assembly of a clathrin (Cltr) coat on the plasma membrane through sequential recruitment of proteins. The coated membrane bends toward the inside of the cell, recruiting additional membrane-bending factors (Schöneberg *et al.*, 2017) and eventually forming an invagination that is only connected to the bulk plasma membrane by a small neck. At this stage, the GTPase dynamin2 (Dnm2) is recruited to the neck and cleaves it. The freed clathrin-coated vesicle is then further internalized and uncoated for processing. Using genome-engineered human embryonic stem cells, we have previously shown that CME dynamics is highly adapted to the needs of different cell types (Dambournet *et al.*, 2018). Over the past few decades, CME studies have been focused on the ventral part of the cell nearest the coverslip surface, which can be accessed easily by total internal reflection fluorescence microscopy (TIRFM). Recent studies started to access the dorsal part of cells grown on coverslips (Aguet *et al.*, 2016) and investigated CME in polarized cells such as Madin–Darby canine kidney (MDCK) cells adherent to a surface (Boulant *et al.*, 2011). Most recently, CME was investigated in migrating cells (Kurl *et al.*, 2015), in live 3D fruitfly embryos (Ferguson *et al.*, 2016), in native 3D zebrafish tissue of nonpolarized cells, and in organoids (Liu *et al.*, 2018).

The tools of 4D cell biology allow us, for the first time, to investigate CME in a well-controlled 3D human polarized-tissue context. First, we engineered human embryonic stem cells to express fluorescent protein–tagged versions of the critical CME proteins Cltr and Dnm2 from their endogenous genomic loci and at endogenous protein levels (Figure 1A, i and ii). Cells were differentiated into 3D intestinal epithelial organoids (Figure 1Aiii) that allow the cells to be observed in their self-assembled 3D architecture. AO-LLSM imaging (Figure 1B) revealed the full dynamics of the CME process throughout the 3D structure of the undisturbed organoids. In particular, it allowed us to investigate protein dynamics simultaneously at all membranes of a cell within a 3D organoid. Finally, we developed and used pyLattice for data analysis and quantification (Figure 1C) to reveal CME dynamics at apical, lateral, and basal membranes. The developed pipeline for data analysis and the pyLattice package are open source and freely available.

RESULTS AND DISCUSSION

Clathrin (Cltr) and dynamin2 (Dnm2) were endogenously tagged with TagRFP and eGFP, respectively, in hESCs (Figure 2A). hESCs were differentiated into 3D intestinal epithelial organoids (Forster *et al.*, 2014). In this protocol, hESCs were cultured to confluence and then injected subcutaneously into immune-compromised mice for teratoma development. Grown teratomas were harvested after 6–8 wk and embedded into undiluted Matrigel droplets in media conditioned with intestinal growth factors (Wnt3a, epidermal growth factor [EGF], Noggin, R-Spondin-1 [WENR]) for 1 wk to develop intestinal epithelial organoids. These organoids can be differentiated into all major cell types by reducing Wnt3a in the media and by the addition of DAPT. However, when cultured in media with high concentrations of Wnt3a, the organoids can be passaged long-term, and they consist of a single layer of intestinal epithelial cells comprising mostly adult stem/progenitor cells with a low frequency of spontaneous differentiation (Forster *et al.*, 2014). The organoids assume the form of a cystic sphere that surrounds a fluid-filled lumen (Figure 2B). Intestinal epithelial cells within the organoids are highly polarized with an actin cortex on the apical membrane and microvilli characteristic of the intestinal brush border (Forster *et al.*, 2014). Moreover, the intestinal nature of these organoids was confirmed by transcriptional profiling (Forster *et al.*, 2014). For each cell, three membrane classes can be defined: the apical (lumen-facing) side, the basal (outside-facing) side, and the lateral membranes that separate cells from each other in the organoid (Figure 2C).

Lattice light-sheet imaging with adaptive optics (AO-LLSM; Liu *et al.*, 2018) was used to reveal the 4D dynamics of CME in the live organoids. The large 3D field of view ($68 \times 58 \times 40$ µm, *xyz*; pixel size 0.097 µm in *xy*, 0.2 µm in *z*) allowed us to image through the organoid's epithelial cell layer (Figure 2D) and to capture Cltr and Dnm2 dynamics on apical, basal, and lateral membranes with a frame rate of 2.85 s/frame per channel. The field of view allowed the simultaneous observation of multiple cells at a time (36 cells in Figure 2E). Punctate structures, corresponding to clathrin-coated vesicles and Dnm2 accumulations, were visible throughout the tissue layer in all three dimensions (Figure 2, F–K). An overlay of the puncta revealed structures that contained both Cltr and Dnm2 (Figure 2, J and K). Apical and basal membrane and nuclear envelope were not specifically labeled, but could be retrieved from the data using image processing (see *Materials and Methods*). Movies of CME dynamics were generally acquired for up to 400 s (70 frames). Imaging at such high frame rates in 4D brings about unique data-handling and image-processing challenges, with file sizes of ~400 MB/frame/channel and movie sizes reaching ~56 GB. Even drastically cropped versions of movies (1%) could not be processed using commercial (e.g., Imaris [Bitplane]) or free (e.g., TrackMate [Tinevez *et al.*, 2017] or llsmtools [Aguet *et al.*, 2016]) software, as the programs would crash, freeze, or demand major customization.

We developed pyLattice, a library of custom image and data analysis tools, to handle the challenge of big data image analysis brought about by high-content 4D imaging technology such as LLSM. In the case of CME, the data analysis task is as follows: input a 4D organoid movie, detect the CME events in that movie, differentiate the events according to their origin membrane (apical, basal, lateral), and perform a statistical analysis of the events (intensity, lifetime, etc.). Algorithmically, this task can be broken into the following parts (Figure 3A): 1) preprocess and input a 4D AO-LLSM movie, 2) detect diffraction-limited Cltr and Dnm2 spots in 3D for every frame, 3) track detected spots over time, 4) match tracks from both channels to each other, and 5) process (filtering, statistical analysis) and 6) visualize the data.

PyLattice was designed with the following principles in mind:

1. Accessibility: as LLSM imaging and other big data imaging techniques become more widespread, more researchers will need access to adequate LLSM image analysis solutions. To remove the two most frequently encountered accessibility barriers (use of a not–widely used programming language and use of expensive proprietary software), we committed ourselves to using Python (van Rossum, 1995), one of the most popular programming languages, for the library. For 4D visualization, the library interfaces with the free and open-source renderer ChimeraX (Goddard *et al.*, 2018). PyLattice itself is open source and freely available under BSD 3-clause license on github (https://github.com/JohSchoeneberg/pyLattice).
2. Interactivity: scientific image analysis requires the user to sample different parameters (signal threshold, tracking search radius, gap length, etc.) and different plotting options to find the best solution for retrieving information from his/her data. PyLattice uses Jupyter notebooks (Perez and Granger, 2007) that contain both input (Python code) and output (computation results, plots) in an intuitive way that facilitates interactivity and sampling.

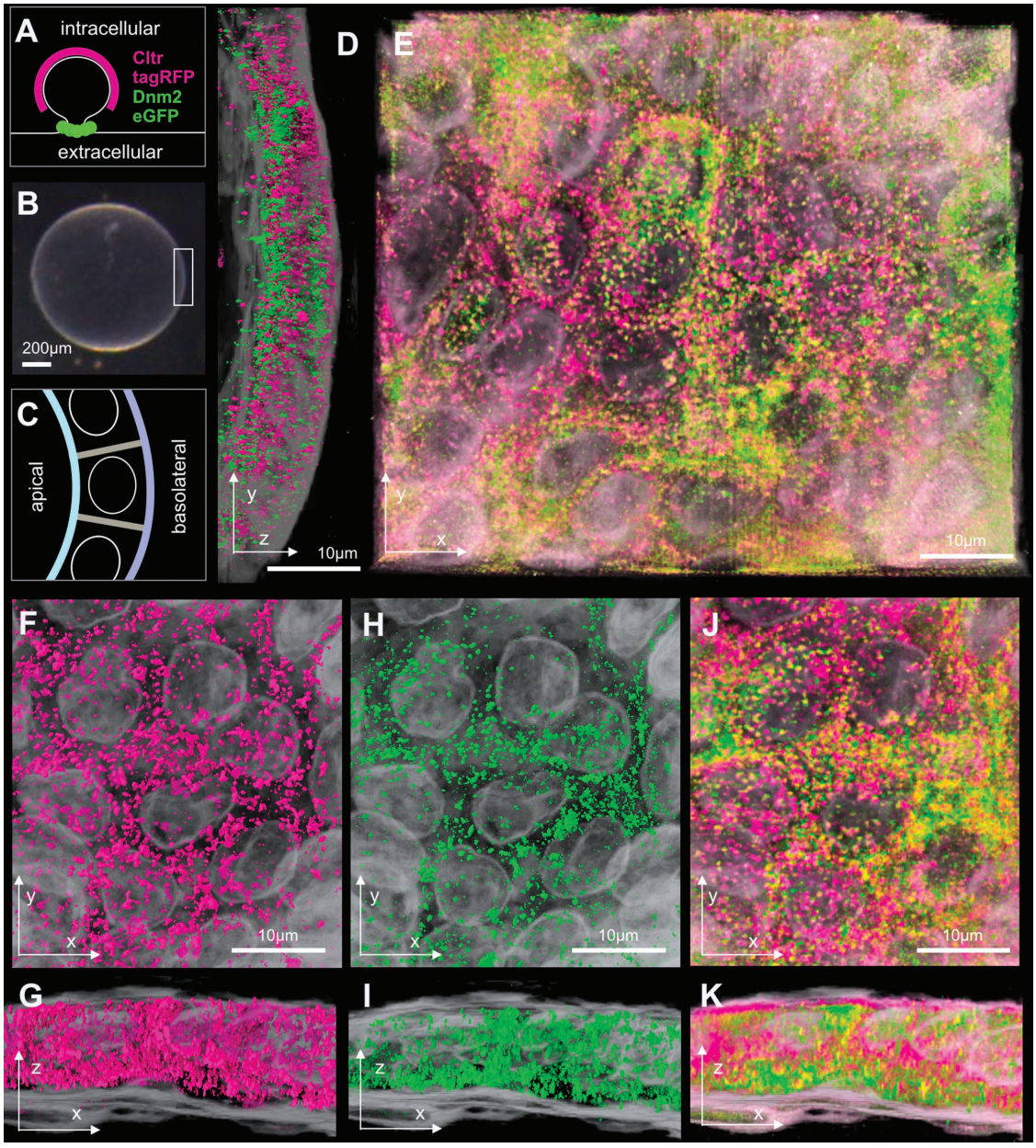

FIGURE 2: 4D AO-LLSM imaging of clathrin (Cltr) and dynamin2 (Dnmz) in intestinal epithelial organoids. (A) Schematic of clathrin-mediated endocytosis (CME) budding the cell membrane (white) inward. Major CME proteins Cltr (magenta) and Dnm2 (green) were endogenously labeled by genome editing in human embryonic stem cells (hESCs) to monitor CME. (B) hESCs were differentiated and grown into intestinal epithelial organoids that assume a spherical appearance with a single layer of cells surrounding a fluid-filled lumen. (C) Schematic of an organoid surface depicting the three plasma membrane classes that can be differentiated: apical (cyan), lateral (gray), and basal (blue). (D–K) Adaptive optics lattice light-sheet (AO-LLSM) imaging of organoids results in high-resolution 4D data (three space dimensions + time) of live tissue and CME dynamics. (D) Side view of a 3D volume that contains part of an organoid cell layer depicting Cltr (magenta) and Dnm2 (green) puncta and the organoids' limiting membranes (gray). (E) Top view of the same 3D volume as depicted in (D), showing Cltr (magenta), Dnm2 (green), and overlapping (yellow) puncta and nuclear envelopes (gray). Shown is a full 3D volume with all internal intensities half transparent. (F–K) Close-up view of Cltr (magenta) and Dnm2 (green) puncta distribution in the tissue in top view (F, H, J) and side view (G, I, K) reveals a wide distribution of Cltr in the interior of the cell (no density in nuclei) due to its widespread involvement in intracellular trafficking. (J, K) Multiple sites exhibit colocalization of Cltr and Dnm2 (yellow), marking the sites of interest for this study.

3. Reusability: we aim to reduce redundancy by reusing as much existing code as possible. For detection, tracking, and matching (tasks 2–4), the Matlab package llsmtools (Aguet *et al.*, 2016) was used as a core, which itself builds on the u-track package (Jaqaman *et al.*, 2008). A Matlab wrapper was written around llsmtools to generalize it and form an interface that seamlessly integrates with the Python/Jupyter library (see *Materials and Methods*).
4. Generalizability: pyLattice is written to be usable beyond the task at hand (AO-LLSM imaging of CME) and should be easily adaptable to any general problem of 4D particle tracking in

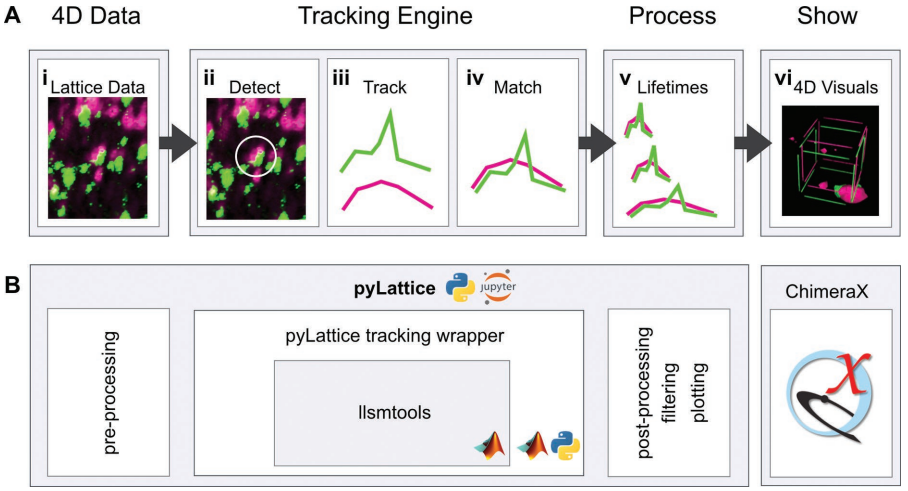

FIGURE 3: 4D image analysis and particle tracking in pyLattice. (A) pyLattice is a library of Python modules, Jupyter notebooks, and Matlab routines that operate together to form an image analysis pipeline. The pipeline steps are as follows (left to right): input of a two-channel 4D AO-LLSM data set (Cltr magenta, Dnm2 green), detection of diffraction-limited puncta, tracking puncta over time, matching each channel's tracks to one another, processing and filtering the resulting set of tracks, and finally visualizing the data. (B) Implementation diagram of pyLattice. Python-based functionality is implemented for data pre- and postprocessing, filtering, quality control, plotting, and tracking. A Matlab wrapper has been created to incorporate llsmtools (Aguet *et al.*, 2016) into the pipeline. 4D visualization is done using ChimeraX, for which pyLattice provides customized visualization input.

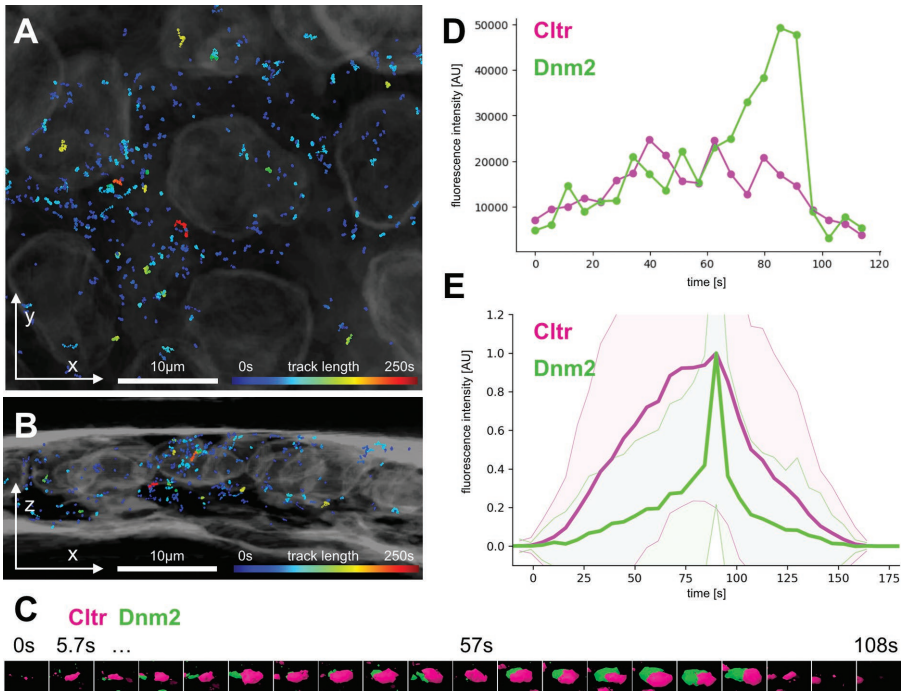

FIGURE 4: Tracking individual clathrin-mediated endocytosis events in 4D. (A) Top view of individual CME events (pseudocolored by lifetime) tracked in the organoid tissue. Most tracks have lifetimes between 35 and 70 s (see Figure 5). (B) A side view of the same tissue section reveals that tracks are found throughout the tissue. (C) Frame-by-frame depiction of a single endocytosis event (Cltr magenta, Dnm2 green, 5.7 seconds per frame, punctum size corresponds to intensity; see also Supplemental Figure S4). (D) Intensity-over-time plot of the event in C. First a clear rise in both Cltr and Dnm2 intensity can be seen. A sharp peak in Dnm2 then precedes the decline in both Cltr and Dnm2 intensity before the track ends. (E) Normalized intensity over time plot of tracks that belong to the same lifetime cohort as the track depicted in D (70–105 s, $N = 330$, shaded area = SD).

LLSM data sets. In addition, pyLattice should be extendable to incorporate additional classes of LLSM image analysis solutions (e.g., membrane trafficking) in the future.

PyLattice provides tools for LLSM input data preprocessing (step 1) such as Jupyter notebook data visualization, movie cropping, and bleaching correction (see Supplemental Figure S1). To ensure accuracy, particle detection, tracking, and matching are each individually interfaced with Jupyter notebooks to allow the user easy access to intermediate results for quality control (see Supplemental Figure S2). Jupyter notebooks for the final analysis step (step 5) enable assignment of CME events to apical, lateral, and basal membrane regions and track classification according to lifetime, as well as various plotting and 4D visualization functionalities (see Supplemental Figure S2). See Supplemental Table S1 for a list of all Jupyter notebooks provided in pyLattice. The online distribution of pyLattice includes the code as well as installation instructions and a manual.

Using pyLattice, CME events were tracked in full 70-frame movies, resulting in ~10^4–3×10^4 raw tracks per movie. To distinguish CME events from other events in the cell, which, for example, involve Cltr alone, only those tracks that showed both a clear Cltr and a clear Dnm2 signal were kept, which represented ~15–30% of the tracks. We note that because our image data include the full volume of the cell, this filtering step eliminated from our analysis non-CME Cltr structures that originated on internal cellular membranes. CME tracks were found throughout the tissue and varied in lifetime (Figure 4, A and B). Individual tracks showed the characteristic behavior of CME: the appearance of a small fluorescent Cltr spot was followed by an increase in Cltr intensity over tens of seconds until a sharp spike in Dnm2 intensity was recorded that marked the scission of the vesicle (see Figure 4, C and D). When multiple tracks of the same lifetime cohort (e.g., 70–105 s, $N = 330$) were gathered and averaged, the pattern of vesicle formation, Dnm2 assembly, scission from the membrane, and uncoating became clearly visible (Figure 4E).

AO-LLSM imaging allowed us to track clathrin-coated vesicles after membrane scission occurred. After the Dnm2 spike, our recordings revealed a quick drop in both Dnm2 and Cltr intensity close to background levels, within less than 10 and 40 s, respectively. While the Dnm2 intensity decreased sharply, the Cltr intensity decrease was more gradual. Using the Dnm2 spike as

a marker for vesicle scission, we determined that about two-thirds of a track's lifetime is spent in vesicle formation and coat assembly and the remaining third in disassembly and uncoating.

To investigate CME on a tissue scale, we tracked all CME events through the full cell layer of four intestinal organoids, comprising ~60 cells per condition (Figure 5). In two control organoids (Figure 5, A and B), out of 29,474 and 16,002 raw tracks, CME events were identified as those showing both Cltr and Dnm2 fluorescence. The resulting 4484 and 3654 tracks were assigned to their origin membrane surfaces (1330 and 1449 basal; 1138 and 1201 lateral; 2016 and 1004 apical) based on each track's start coordinates (see *Materials and Methods*). The lifetime distributions for each track class were almost identical and did not display a difference by origin membrane (Figure 5, C and D). Tracks were further classified by lifetime cohort, with the first cohort comprising all tracks lasting 0–34 s, the second cohort comprising tracks from 34 to 68 s, and so on (Figure 5, C and D, insets). The largest fraction of tracks (~40–50%) were found to last between 34 and 68 s. The second most prevalent fraction were tracks of the adjacent lifetime cohorts (0–34 s, ~15–20%; 68–10 s, ~20–25%). Only ~8–16% of all tracks lasted longer than 102 s. Investigating the lifetime cohorts with regard to the fluorescence intensity dynamics (Figure 5, E–J) revealed that the overall shape of a CME event is consistent through all lifetime cohorts: an increase in Cltr intensity is followed by a Dnm2 peak, ending with quick intensity decreases of both Cltr and Dnm2. For each subsequent lifetime cohort, the peak intensity of both Cltr and Dnm2 increased relative to the preceding cohort (by 22 ± 10% for Cltr and 81 ± 10% for Dnm2), indicating that more molecules are recruited to these respective sites. We found that this pattern is remarkably consistent: fluorescence intensities and lifetime dynamics of CME on apical membranes (Figure 5, E and F) very closely matched readouts from lateral (Figure 5, G and H) and basal (Figure 5, I and J) membranes.

Molecules that interfere with the actin cytoskeleton are known to change the dynamics of CME and have been reported to act asymmetrically on membranes of polarized cells (Boulant *et al.*, 2011). We incubated organoids for 10 min with the actin-stabilizing drug Jasplakinolide (JASP). Imaging and data processing for two independent Jasplakinolide-treated organoids resulted in 3322 and 2991 tracks (from 13,669 and 10,735 raw tracks) that could be assigned to their origin membranes (1249 and 1171 basal; 1285 and 1131 lateral; 788 and 689 apical; Figure 5, K and L). Lifetime analysis (Figure 5, M and N) revealed that the lifetimes are similar to each other and to the control condition. Cohort populations were similar to the control condition, with the predominant fraction of tracks (~50%) falling in the 34–68 s cohort (Figure 5, M and N insets). When shapes of the CME dynamics profiles are compared between control and treatment conditions (Figure 5, E and F vs. O–T), it is notable that the dynamics (the shapes of the Cltr and Dnm2 recruitment profiles) behaved almost identically. From results in MDCK cells (Boulant *et al.*, 2011), the apical membrane would have been expected to show tracks that were drastically shifted toward longer lifetimes. While we see apparent effects of the JASP treatment, such as fewer total apical tracks (Figure 5U), lower overall Cltr fluorescence intensity (Figure 5V), and a changed Dnm2 fluorescence intensity profile of apical and basal tracks (Figure 5W), Cltr pits with longer lifetimes could not be identified in either the processed tracks or the raw tracks before processing. When the rate of fluorescence change was investigated between lifetime cohorts (cohort 1 vs. cohort 4), longer-lifetime cohorts consistently showed increased fluorescence. While this fluorescence increase was consistent among apical, lateral, and basal membranes under the control condition (33 ± 8% Cltr, 63 ± 15% Dnm2), under JASP treatment the increase was strongly dependent on the membrane compartment (Figure 5X). Dnm2 fluorescence increased more on the basal membrane (102 ± 3%) and increased less on the apical membrane (52 ± 12%), indicating a possible redistribution of Dnm2 to counteract an asymmetric effect of the drug.

In this study, we succeeded in determining CME lifetime distributions in two colors for three separate membrane domains of each cell in large volumes containing ~35 cells in intact tissue. To obtain these results, we combined endogenous genome editing in human stem cells, intestinal epithelial organoid formation, AO-LLSM microscopy, and big data image analytics to study CME in cells organized into tissues instead of grown on a surface. Owing to the unique imaging capabilities of the AO-LLSM, we could for the first time simultaneously image both Cltr and Dnm2 dynamics on all three plasma membrane domains (apical, lateral, and basal) in 4D in a human polarized epithelium. We developed the novel LLSM image analysis framework pyLattice to analyze the large LLSM data sets and retrieve CME dynamics.

How growth of cells in a 3D organoid context would affect CME dynamics relative to what had been observed for cells grown on glass was not known. The lifetime distributions in organoids for clathrin-coated vesicle formation in all three membrane domains, apical, lateral, and basal, is very close to published values for apical and basal membranes in MDCK polarized cells (Boulant *et al.*, 2011). In addition, fluorescence intensity dynamics for Cltr and Dnm2 followed profiles similar to those observed for cells grown on glass: Cltr slowly increases to a plateau in fluorescence intensity. Once a neck has formed, Dnm2 assembles around the neck, resulting in a peak in Dnm2 fluorescence when the vesicle is cut off from its origin membrane. While other techniques such as TIRFM cannot follow newly released vesicles past this scission event, using AO-LLSM we could follow the vesicles further until they were uncoated. Importantly, we observed that the time fractions spent in coat assembly and uncoating were roughly 2/3 and 1/3, respectively. We found little to no difference in lifetimes or fluorescence intensity profiles when CME events were classified with respect to origin membrane (apical, lateral, basal). This observation is consistent with findings for adherent polarized MDCK cells (Boulant *et al.*, 2011) and adherent single nonpolarized cells (Aguet *et al.*, 2016).

Next, we applied the actin cytoskeleton–stabilizing drug JASP. Similar lifetimes were still observed across all membranes. This observation was somewhat surprising, given reported actin dependence of efficient vesicle formation on the different membranes (Yarar *et al.*, 2005; Boulant *et al.*, 2011; Cheng *et al.*, 2012; Grassart *et al.*, 2014; Dambournet *et al.*, 2018). Other studies had found that JASP alters CME dynamics, shifting CME events to much longer lifetimes and stalling them (Grassart *et al.*, 2014). In adherent MDCK cells, such CME-arresting effects were observed, but notably only for the apical membrane (Boulant *et al.*, 2011). Interestingly, tracks originating from the apical membrane showed a marked change in response to JASP: the Dnm2 fluorescence increase for longer tracks was much smaller, while the same increase was much larger for the basal membrane. This observation may reflect a cellular response of recruiting more/fewer Dnm2 molecules to CME sites in an environment of asymmetrically changed actin assembly due to JASP. One possible explanation for the difference between our findings and previous findings in MDCK cells is that our study tracked CME in 3D using two colors of endogenously tagged proteins (Cltr and Dnm2). In the MDCK study (Boulant *et al.*, 2011), the Cltr adaptor protein 2 (AP2) was used as a single marker for endocytosis, potentially displaying different dynamics in response to JASP treatment than Cltr and Dnm2. It is also possible that the different observations are due

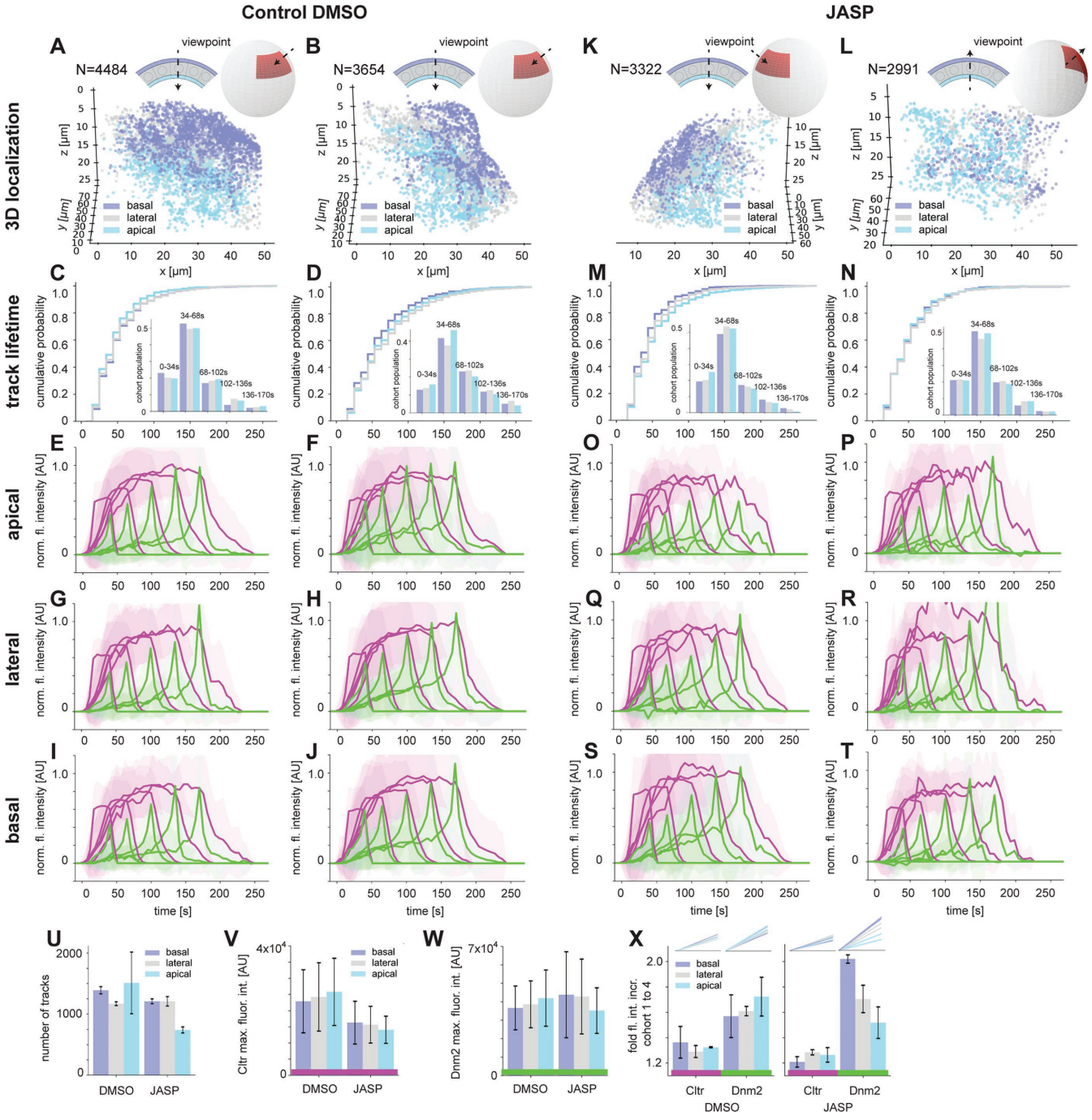

FIGURE 5: Tissue-scale tracking reveals apical, basal, and lateral membrane dynamics of CME in epithelial intestinal organoids. Two cases were compared, a dimethyl sulfoxide (DMSO) control, A–J, and a 10-min Jasplakinolide (JASP) treatment, K–T. (A, B, K, L) Three-dimensional depiction of the detected tracks through the organoid's epithelial layer. We classified tracks by origin membrane into apical (cyan), lateral (gray), and basal (blue). Red tiles on a sphere serve as a guide from whose viewpoint the organoid is depicted. Lower-lying tracks can be seen when not obstructed by higher-lying tracks. (C, D, M, N) Cumulative lifetime plots for the tracks. The inset depicts a normalized distribution of the tracks in subsequent 34-s lifetime cohorts. (E–T) Average fluorescence intensity of Cltr (magenta) and Dnm2 (green) for each lifetime cohort over time; shaded area = SD. (U) Comparison of the total number of tracks for each membrane class in DMSO (control) and JASP treatment. (V, W) Peak intensity distribution of Cltr and Dnm2 differentiated by membrane class. (X) Fold fluorescence increase from cohort 1 to cohort 4 in both DMSO control and JASP treatment shows an asymmetric change for JASP. (Bars = mean ± SD; in W, 0.5 × SD is depicted for visual clarity.)

to the use of different cell types and conditions, but this leaves open the question of whether the JASP fully penetrated the organoids in our studies.

The quantitation and analysis of imaging data and Cltr dynamics was made possible by the custom image analysis package pyLattice. The advent of high-content big data–imaging modalities such

as AO-LLSM will make gigabyte movies and terabyte data sets the standard. Automated image analysis provides hope for quantitating such enormous data sets, as manual and semimanual analysis is no longer practical on such scales. pyLattice was conceived with generalizability and ease of use in mind so that it could be applied not only to CME but also to all tasks that involve tracking punctate structures in LLSM images. Closer ties between biologists, microscopists, data scientists, and computer scientists will allow the development of additional algorithms that can be incorporated into existing libraries. We predict that, driven by the scale of the data sets, these tools will create higher demands for computational power and resources and will run on dedicated workstations or clusters. This study shows how a confluence of technologies from stem cell biology, 3D organoid culture, advanced microscopy, and big data image analytics can open the door for tissue-scale 4D quantitative cell biology.

MATERIALS AND METHODS

Genome-engineered intestinal epithelial organoids

Cell culture. hESCs (WIBR3, NIH stem cell registration 0079) were cultured as described (Soldner *et al.*, 2009; Hockemeyer *et al.*, 2011). Briefly, hESCs were maintained on a layer of inactivated mouse embryonic fibroblast (MEFs) in hESC medium (DMEM/F12 (Lifetech)) supplemented with 20% KnockOut Serum Replacement (Gibco 10828028), 1 mM glutamine (Gibco 25030-081), 1% nonessential amino acids (Gibco 11140076), 0.1 mM β-mercaptoethanol (Sigma-Aldrich M6250), 1000 U/ml penicillin/streptomycin (Gibco15140122), and 4 ng/ml FGF-Basic full (Invitrogen PHG0263). Cultures were passaged every 7 d with 1.5 mg/ml collagenase type IV (Gibco 17104019) and gravitational sedimentation by washing three times in wash media (DMEM/F12 [Gibco 11320- 033]) supplemented with 5% fetal bovine serum (Gibco 10437028) and 1000 U/ml penicillin/streptomycin (Gibco 15140122).

Genome editing. The CLTA genes were targeted as previously described using a paired ZFN that targets exon 7 and cuts precisely at the stop codon (Doyon *et al.*, 2011; Hong *et al.*, 2015). Design of donor plasmids and ZFNs was described previously (Doyon *et al.*, 2011). The *DNM2* gene was targeted in exon 22 using CRISPR/Cas9 and cctgctcgactaggcctcga as single guide RNA (sgRNA) target site for Cas9, and sgRNAs were expressed using the pX330 plasmid (Addgene plasmid 42230; Cong *et al.*, 2013; Ran *et al.*, 2013). hESCs ([1–2] $\times 10^7$) were electroporated with 5 μg of each ZFN (or 10 μg of pX330 Cas9 plasmid) and 40 μg of repair donor plasmid. Cells were sorted for expression of GFP and/or TagRFP fluorescence 72 h after electroporation. Clonal populations were isolated and characterized as described (Dambournet *et al.*, 2014).

Generation of intestinal epithelial organoids. Intestinal organoids were derived for genome-engineered hESCs as described previously (Forster *et al.*, 2014). Briefly, genome-engineered hESCs were injected subcutaneously into NOD-SCID mice (Taconic). Teratomas (<2 cm) formed within 6–8 wk were isolated and disaggregated into a single-cell suspension, and ~5×10^4 cells were embedded in 50 μl Matrigel (Corning 354234) in a well of a 24-well plate. Cells were incubated at 37°C for 15 min, and after the Matrigel solidified, growth medium (see below) was added to the well. Organoids formed over the period of a week before cultures were passaged by 30 min dissociation in Dispase (5 U/ml; Stemcell Technologies) and gravity sedimentation of newly forming organoids (3 × 2 min at 40 × *g* in 12.5 ml of DMEF12 (Gibco 11320-033) with 0.5% bovine serum albumin (BSA) (Sigma; A4503)). Single cells were aspirated with the supernatant of each wash to mechanically enrich for the faster-sedimenting organoids. This procedure resulted in almost homogeneous organoid cultures after three passages over three 1-wk intervals. Subsequent passages were done by mechanical shearing with a P1000 pipette after 5 min exposure to 2 mM EDTA, 0.5% BSA in PBS.

Organoid culture medium. Organoids were cultured using conditioned medium products as previously described (Forster *et al.*, 2014). Low-passage L-WRN cells (producing Wnt-3A, R-spondin 1, and noggin) were cultured as described previously (Miyoshi and Stappenbeck, 2013; Forster *et al.*, 2014) in DMEM with high glucose (Sigma; D6429) supplemented with 10% fetal bovine serum, 50 mg/ml G418 (Gibco 11965-092), and 100 mg/ml hygromycin (Millipore Sigma 400050) to confluence and passaged 1:4. When confluent again, 20 ml of new medium per 150 cm^2 flask comprising Advanced DMEM/F12 (Life Technologies 12634010), 200 mM L-glutamine (Gibco 25030-081), 10,000 U/ml penicillin, and 10 mg/ml streptomycin (Gibco 15140122) and 0.5% BSA (Sigma; A4503) was added and collected each day for 4 d and stored at 4°C before filtration and freezing. This conditioned base medium was supplemented 1:1 with a volume of unconditioned base medium comprising Advanced DMEM/F-12 (Gibco 12634010), N2 (Gibco 17502-048), B27(Gibco 12587-010), L-glutamine (Gibco 25030- 081), 10,000 U/ml penicillin and 10 mg/ml streptomycin (Gibco 15140122), nonessential amino acids (Gibco 11140076) and stored in frozen aliquots. Immediately before use, the medium was supplemented with EGF (50 ng/ml; R&D Systems 236-EG-01M) and added into the well containing Matrigel (Corning 47743-716)-embedded organoids. Two days before imaging, organoids were released by Dispase (5 U/ml; Stemcell Technologies) digestion and resuspended in 10–20 μl Matrigel without phenol red (Corning 47743-716), placed at 4°C on a 5 mm–diameter coverslip (Warner Instruments 64-0700), and incubated at 37°C before medium was added. Medium was replaced with DMEM/F12 without phenol red (Life Technologies 21041025) with 10 mM HEPES (Gibco 15630080) for imaging.

Lattice light-sheet imaging with adaptive optics

The imaging of the organoids was carried out using the AO-LLSM from the Betzig laboratory at the Howard Hughes Medical Institute Janelia Research Campus (Ashburn, VA). Before data acquisition, sample-induced aberration was measured via direction wavefront sensing though both the excitation and detection objectives. Light from a Ti:Sapphire ultrafast pulsed laser (Coherent Cameleon Ultra II) was ported to either the excitation or the detection arm. Two photon–excited fluorescence generated within the specimen by scanning the guide star focused by excitation or detection objective was collected by the same objective, descanned (Wang *et al.*, 2014), and sent to a homebuilt Shack–Hartmann wavefront sensor consisting of a square microlens array (Edmund Optics) focused onto an electron-multiplying (EM) CCD camera (Andor iXon).

The light sheet was generated using a square lattice configuration in dithered mode (Chen *et al.*, 2014) with the corrective wavefront applied to the space-light modulator (Holoeye Pluto BB). The 3D objects were imagined by scanning the objective and the dithered light sheet at 200-nm step sizes in the *z*-axis, thereby capturing a volume of ~70 × 60 × 40 μm every 2.48–2.85 s. Each plane of the imaged volume was exposed for 20–30 ms and excited using either a 488-nm laser (for eGFP) or a 560-nm laser (for TagRFP, both lasers from MPB Lasers) at 50–60 μW with an excitation NA of 0.517/0.55 and a corresponding light-sheet length of 30 μm. The fluorescence signal was first reflected by a deformable mirror

(ALPAO 97-15) loaded with corrective wavefront and then acquired with a Hamamatsu ORCA-Flash 4.0 scientific complementary metal oxide semiconductor (sCMOS) camera.

pyLattice and data processing

pyLattice. pyLattice builds on llsmtools (Aguet *et al.*, 2016), a Matlab toolbox that extends u-track (Jaqaman *et al.*, 2008), to do tracking in the 3D context of LLSM data sets. The core functionality of llsmtools has been retained and forms the detection and tracking routines of pyLattice. llsmtools' project-specific routines for single-cell LLSM data (Aguet *et al.*, 2016) and its input/output functionality has been replaced by a more general Matlab wrapper that also forms the interface to the Python/Jupyter layers of the pyLattice library. The Python/Jupyter layer of the package consists of 25 Python Classes/Jupyter Notebooks that handle 1) AO-LLSM data preprocessing such as bleaching correction or data cropping, 2) quality control for the detection and tracking pipeline, 3) data postprocessing such as track classification by length, intensity, and origin in space, 4) project-specific tasks such as label-free membrane identification (see below) or the identification of apical, lateral, and basal tracks (see below), and 5) result visualization and plotting, such as 3D track visualization or, lifetime cohort plots. See the software distribution on github for a more detailed description, the pyLattice package itself, training data, and usage/installation instructions.

Puncta detection and tracking. Experimentally measured point spread functions are used for a wavelet transformation of the lattice data, resulting in a set of 3D candidate coordinates for each frame. Candidate coordinates that lie above background are fitted to a 3D Gaussian model to retrieve position and amplitude for each punctum. For tracking, puncta are first linked to each other frame by frame using a cost-matrix approach. This cost matrix is then used in a subsequent step to globally perform track merging, termination, and gap closing operations. For details, see Jaqaman *et al.* (2008) and Aguet *et al.* (2016).

Track postprocessing. The reporter proteins used for CME, Cltr, and Dnm2 take part in different, non-CME-related processes in the cell. To differentiate CME events from other events, 1000 tracks were manually classified as CME tracks if the tracks showed significant signal in both the Cltr and Dnm2 channels and if the tracks ended with Dnm2 peaks. From this classified set, an automated classifier was developed that could reproduce the manual classification with 85% accuracy when it included all tracks in which the Dnm2 peak intensity was high compared with Cltr peak intensity (max_Cltr/max_Dnm2 < 1.5) and in which the Dnm2 peak occurred after half of the track's lifetime (time(max_Dnm2)/track_lifetime > 0.5). Throughout the postprocessing, we ensured that all genuine CME tracks were retained and only separated from noise and non-CME tracks.

Definition of apical, lateral, and basal tracks. Fluorescence signals of Dnm2 and Cltr originate only from within the epithelial cell layer of the organoid. This 3D fluorescence intensity band is used to calculate a 2D surface (middle surface) that resides in the middle of the organoid's cell layer, in between the apical and basal membranes. Depending on the thickness of the organoid's cell layer, margins are defined that classify every track that originates above the middle surface plus margin as an apical track, every track that originates below the middle surface minus margin as a basal track, and every track in between as a lateral track.

Interface to ChimeraX for visualization and quality control. ChimeraX comes with excellent 4D data-viewing capabilities. For this study, visualization and quality control demanded additional functionality, such as 1) display of cropped subsets of the AO-LLSM data, 2) display of detected puncta, and 3) display of detected tracks. For each task, custom functionality has been developed: pyLattice contains Jupyter notebooks that have been designed to process AO-LLSM data sets and pipeline outputs (such as detection or tracking coordinates) and to write files that can be imported into ChimeraX for display.

Label-free identification of nuclear envelope and organoid apical/basal membrane. The nuclear envelope and the apical and basal membranes of the organoid were not specifically labeled, but their positions could be extracted from information contained in the fluorescence localization data from the labeled proteins (Cltr, Dnm2). The outside of the organoid, as well as the inside of the nucleus, is free of labeled proteins. The fluorescence intensity of a labeled protein was inverted and subsequently a threshold was applied that traces the rim of the spaces with absent fluorescence. The result is a 3D map of voxels that outline the nuclear envelope as well as both epithelial surfaces (apical and basal) of the organoid. As intestinal epithelial organoids are spherical, the curvature of the cell layer allows the identification of the apical membrane (lumen-facing, negative curvature) and basal membrane (outward-facing, positive curvature).

ACKNOWLEDGMENTS

Molecular graphics and analyses were performed with UCSF ChimeraX, developed by the Resource for Biocomputing, Visualization, and Informatics at the University of California, San Francisco (supported by National Institute of General Medical Sciences P41-GM103311). J.S. acknowledges a Moore/Sloan Data Science Fellowship from the Berkeley Institute for Data Science and a Siebel Fellowship from the Siebel Stem Cell Institute–UC Berkeley. This work was supported by National Institutes of Health (NIH) Grant R35GM118149 to D.G.D. D.H. is a Pew–Stewart Scholar for Cancer Research supported by the Pew Charitable Trusts and the Alexander and Margaret Stewart Trust. D.H. is supported by the Siebel Stem Cell Institute and NIH R01-CA196884.

REFERENCES

Aguet F, Upadhyayula S, Gaudin R, Chou Y-Y, Cocucci E, He K, Chen B-C, Mosaliganti K, Pasham M, Skillern W, *et al.* (2016). Membrane dynamics of dividing cells imaged by lattice light-sheet microscopy. Mol Biol Cell 27, 3418–3435.

Barker N, van Es JH, Kuipers J, Kujala P, van den Born M, Cozijnsen M, Haegebarth A, Korving J, Begthel H, Peters PJ, *et al.* (2007). Identification of stem cells in small intestine and colon by marker gene Lgr5. Nature 449, 1003–1007.

Boulant S, Kural C, Zeeh J-C, Ubelmann F, Kirchhausen T (2011). Actin dynamics counteract membrane tension during clathrin-mediated endocytosis. Nat Cell Biol 13, 1124–1131.

Cheeseman BL, Günther U, Susik M, Gonciarz K, Sbalzarini IF (2018). Forget pixels: adaptive particle representation of fluorescence microscopy images. bioRxiv 263061.

Chen BC, Legant WR, Wang K, Shao L, Milkie DE, Davidson MW, Janetopoulos C, Wu XS, Hammer JA, Liu Z, *et al.* (2014). Lattice light-sheet microscopy: Imaging molecules to embryos at high spatiotemporal resolution. Science 346, 1257998.

Cheng J, Grassart A, Drubin DG (2012). Myosin 1E coordinates actin assembly and cargo trafficking during clathrin-mediated endocytosis. Mol Biol Cell 23, 2891–2904.

Clevers H (2016). Modeling development and disease with organoids. Cell 165, 1586–1597.

Cong L, Ran FA, Cox D, Lin S, Barretto R, Habib N, Hsu PD, Wu X, Jiang W, Marraffini LA, Zhang F (2013). Multiplex genome engineering using CRISPR/Cas systems. Science 339, 819–823.

Crespo M, Vilar E, Tsai SY, Chang K, Amin S, Srinivasan T, Zhang T, Pipalia NH, Chen HJ, Witherspoon M, *et al*. (2017). Colonic organoids derived from human induced pluripotent stem cells for modeling colorectal cancer and drug testing. Nat Med 23, 878–884.

Dambournet D, Hong SH, Grassart A, Drubin DG (2014). Tagging endogenous loci for live-cell fluorescence imaging and molecule counting using ZFNs, TALENs, and Cas9. Methods Enzymol 546, 139–160.

Dambournet D, Sochacki KA, Cheng AT, Akamatsu M, Taraska JW, Hockemeyer D, Drubin DG (2018). Genome-edited human stem cells expressing fluorescently labeled endocytic markers allow quantitative analysis of clathrin-mediated endocytosis during differentiation. J Cell Biol 217, 3301–3311.

Doyon JB, Zeitler B, Cheng J, Cheng AT, Cherone JM, Santiago Y, Lee AH, Vo TD, Doyon Y, Miller JC, *et al*. (2011). Rapid and efficient clathrin-mediated endocytosis revealed in genome-edited mammalian cells. Nat Cell Biol 13, 331–337.

Fatehullah A, Tan SH, Barker N (2016). Organoids as an in vitro model of human development and disease. Nat Cell Biol 18, 246–254.

Ferguson JP, Willy NM, Heidotting SP, Huber SD, Webber MJ, Kural C (2016). Deciphering dynamics of clathrin-mediated endocytosis in a living organism. J Cell Biol 214, 347.

Forster R, Chiba K, Schaeffer L, Regalado SG, Lai CS, Gao Q, Kiani S, Farin HF, Clevers H, Cost GJ, *et al*. (2014). Human intestinal tissue with adult stem cell properties derived from pluripotent stem cells. Stem Cell Rep 2, 838–852.

Goddard TD, Huang CC, Meng EC, Pettersen EF, Couch GS, Morris JH, Ferrin TE (2018). UCSF ChimeraX: meeting modern challenges in visualization and analysis. Protein Sci 27, 14–25.

Grassart A, Cheng AT, Hong SH, Zhang F, Zenzer N, Feng Y, Briner DM, Davis GD, Malkov D, Drubin DG (2014). Actin and dynamin2 dynamics and interplay during clathrin-mediated endocytosis. J Cell Biol 205, 721–735.

Hockemeyer D, Wang H, Kiani S, Lai CS, Gao Q, Cassady JP, Cost GJ, Zhang L, Santiago Y, Miller JC, *et al*. (2011). Genetic engineering of human pluripotent cells using TALE nucleases. Nat Biotechnol 29, 731–734.

Hong SH, Cortesio CL, Drubin DG (2015). Machine-learning-based analysis in genome-edited cells reveals the efficiency of clathrin-mediated endocytosis. Cell Rep 12, 2121–2130.

Jaqaman K, Loerke D, Mettlen M, Kuwata H, Grinstein S, Schmid SL, Danuser G (2008). Robust single-particle tracking in live-cell time-lapse sequences. Nat Methods 5, 695–702.

Kaksonen M, Roux A (2018). Mechanisms of clathrin-mediated endocytosis. Nat Rev Mol Cell Biol 19, 313–326.

Kural C, Akatay AA, Gaudin R, Chen B-C, Legant WR, Betzig E, Kirchhausen T (2015). Asymmetric formation of coated pits on dorsal and ventral surfaces at the leading edges of motile cells and on protrusions of immobile cells. Mol Biol Cell 26, 2044–2053.

Lancaster MA, Knoblich JA (2014). Organogenesis in a dish: modeling development and disease using organoid technologies. Science 345, 1247125.

Liu T-L, Upadhyayula S, Milkie DE, Singh V, Wang K, Swinburne IA, Mosaliganti KR, Collins ZM, Hiscock TW, Shea J, *et al*. (2018). Observing the cell in its native state: imaging subcellular dynamics in multicellular organisms. Science 360, eaaq1392.

McCracken KW, Catá EM, Crawford CM, Sinagoga KL, Schumacher M, Rockich BE, Tsai YH, Mayhew CN, Spence JR, Zavros Y, Wells JM (2014). Modelling human development and disease in pluripotent stem-cell-derived gastric organoids. Nature 516, 400–404.

Miyoshi H, Stappenbeck TS (2013). In vitro expansion and genetic modification of gastrointestinal stem cells in spheroid culture. Nat Protoc 8, 2471–2482.

Ootani A, Li X, Sangiorgi E, Ho QT, Ueno H, Toda S, Sugihara H, Fujimoto K, Weissman IL, Capecchi MR, Kuo CJ (2009). Sustained in vitro intestinal epithelial culture within a Wnt-dependent stem cell niche. Nat Med 15, 701–706.

Ounkomol C, Seshamani S, Maleckar MM, Collman F, Johnson G (2018). Label-free prediction of three-dimensional fluorescence images from transmitted light microscopy. Nat Methods, https://doi.org/10.1038/s41592-018-0111-2.

Perez F, Granger BE (2007). IPython: a system for interactive scientific computing. Comput Sci Eng 9, 21–29.

Ran FA, Hsu PD, Lin CY, Gootenberg JS, Konermann S, Trevino AE, Scott DA, Inoue A, Matoba S, Zhang Y, Zhang F (2013). Double nicking by RNA-guided CRISPR Cas9 for enhanced genome editing specificity. Cell 154, 1380–1389.

Rueden CT, Schindelin J, Hiner MC, DeZonia BE, Walter AE, Arena ET, Eliceiri KW (2017). ImageJ2: ImageJ for the next generation of scientific image data. BMC Bioinformatics 18, 529.

Sato T, Stange DE, Ferrante M, Vries RG, Van Es JH, Van den Brink S, Van Houdt WJ, Pronk A, Van Gorp J, Siersema PD, Clevers H (2011). Long-term expansion of epithelial organoids from human colon, adenoma, adenocarcinoma, and Barrett's epithelium. Gastroenterology 141, 1762–1772.

Sato T, Vries RG, Snippert HJ, van de Wetering M, Barker N, Stange DE, van Es JH, Abo A, Kujala P, Peters PJ, Clevers H (2009). Single Lgr5 stem cells build crypt-villus structures in vitro without a mesenchymal niche. Nature 459, 262–265.

Schindelin J, Arganda-Carreras I, Frise E, Kaynig V, Longair M, Pietzsch T, Preibisch S, Rueden C, Saalfeld S, Schmid B, *et al*. (2012). Fiji: an open-source platform for biological-image analysis. Nat Methods 9, 676–682.

Schöneberg J, Lehmann M, Ullrich A, Posor Y, Lo W-T, Lichtner G, Schmoranzer J, Haucke V, Noé F (2017). Lipid-mediated PX-BAR domain recruitment couples local membrane constriction to endocytic vesicle fission. Nat Commun 8, 15873.

Soldner F, Hockemeyer D, Beard C, Gao Q, Bell GW, Cook EG, Hargus G, Blak A, Cooper O, Mitalipova M, *et al*. (2009). Parkinson's disease patient-derived induced pluripotent stem cells free of viral reprogramming factors. Cell 136, 964–977.

Spence JR, Mayhew CN, Rankin SA, Kuhar MF, Vallance JE, Tolle K, Hoskins EE, Kalinichenko VV, Wells SI, Zorn AM, *et al*. (2011). Directed differentiation of human pluripotent stem cells into intestinal tissue in vitro. Nature 470, U105–U120.

Tinevez J-Y, Perry N, Schindelin J, Hoopes GM, Reynolds GD, Laplantine E, Bednarek SY, Shorte SL, Eliceiri KW (2017). TrackMate: an open and extensible platform for single-particle tracking. Methods 115, 80–90.

van Rossum G (1995). Python tutorial. Technical Report CS-R9526, Centrum voor Wiskunde en Informatica (CWI), Amsterdam.

Wang K, Milkie DE, Saxena A, Engerer P, Misgeld T, Bronner ME, Mumm J, Betzig E (2014). Rapid adaptive optical recovery of optimal resolution over large volumes. Nat Methods 11, 625–628.

Yarar D, Waterman-Storer CM, Schmid SL (2005). A dynamic actin cytoskeleton functions at multiple stages of clathrin-mediated endocytosis. Mol Biol Cell 16, 964–975.